This is an open access article published under a Creative Commons Non-Commercial No Derivative Works (CC-BY-NC-ND) Attribution License, which permits copying and redistribution of the article, and creation of adaptations, all for non-commercial purposes.

ACS APPLIED MATERIALS & INTERFACES

ACS AUTHORCHOICE

www.acsami.org

Research Article

Tuning Cell Behavior on 3D Scaffolds Fabricated by Atmospheric Plasma-Assisted Additive Manufacturing

Maria Cámara-Torres, Ravi Sinha, Paolo Scopece, Thomas Neubert, Kristina Lachmann, Alessandro Patelli, Carlos Mota, and Lorenzo Moroni*

Cite This: https://dx.doi.org/10.1021/acsami.0c19687

Read Online

ACCESS | Metrics & More | Article Recommendations | Supporting Information

ABSTRACT: Three-dimensional (3D) scaffolds with optimum physicochemical properties are able to elicit specific cellular behaviors and guide tissue formation. However, cell−material interactions are limited in scaffolds fabricated by melt extrusion additive manufacturing (ME-AM) of synthetic polymers, and plasma treatment can be used to render the surface of the scaffolds more cell adhesive. In this study, a hybrid AM technology, which combines a ME-AM technique with an atmospheric pressure plasma jet, was employed to fabricate and plasma treat scaffolds in a single process. The organosilane monomer (3-aminopropyl)trimethoxysilane (APTMS) and a mixture of maleic anhydride and vinyltrimethoxysilane (MA-VTMOS) were used for the first time to plasma treat 3D scaffolds. APTMS treatment deposited plasma-polymerized films containing positively charged amine functional groups, while MA-VTMOS introduced negatively charged carboxyl groups on the 3D scaffolds' surface. Argon plasma activation was used as a control. All plasma treatments increased the surface wettability and protein adsorption to the surface of the scaffolds and improved cell distribution and proliferation. Notably, APTMS-treated scaffolds also allowed cell attachment by electrostatic interactions in the absence of serum. Interestingly, cell attachment and proliferation were not significantly affected by plasma treatment-induced aging. Also, while no significant differences were observed between plasma treatments in terms of gene expression, human mesenchymal stromal cells (hMSCs) could undergo osteogenic differentiation on aged scaffolds. This is probably because osteogenic differentiation is rather dependent on initial cell confluency and surface chemistry might play a secondary role.

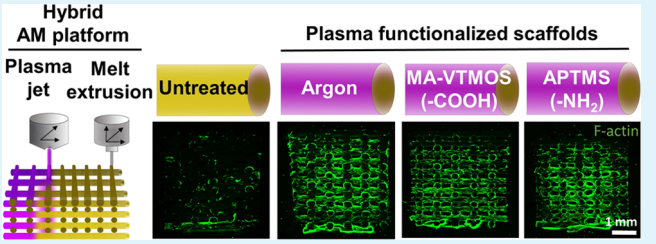

KEYWORDS: *3D scaffolds, melt extrusion additive manufacturing, atmospheric pressure plasma jet, plasma functionalization, human mesenchymal stromal cells, cell adhesion, osteogenesis.*

Downloaded via 151.51.134.59 on January 20, 2021 at 09:51:02 (UTC).
See https://pubs.acs.org/sharingguidelines for options on how to legitimately share published articles.

1. INTRODUCTION

Over the past few decades, additive manufacturing (AM), and in particular melt extrusion AM (ME-AM), has emerged as an advanced fabrication technique for the development of scaffolds for skeletal tissue engineering. This is due to the possibility of producing cost-effective, customizable, biocompatible, and biodegradable three-dimensional (3D) constructs, with interconnected macropores facilitating tissue ingrowth while maintaining sufficient mechanical properties for load-bearing applications.[1] To ensure tissue formation and to obtain reliable readouts when evaluating a scaffold functionality in vitro, an efficient cell attachment upon seeding, in terms of cell density and distribution, is particularly important.[2−4] Moreover, cell colonization also plays a pivotal role in guaranteeing the in vivo success of both cell-laden and cell-free scaffolds. Despite their advantageous structural features, cell adhesion has shown to be challenging on ME-AM scaffolds due to their large pores and lack of biological recognition sites to enable cell−material interactions, as they are mostly made of synthetic thermoplastic polymers, such as poly(ε-caprolactone) (PCL), poly(lactic acid) (PLA), poly(lactic-*co*-glycolic acid) (PLGA), poly(urethane) (TPU), or poly(ethylene oxide terephthalate)/poly(butylene terephthalate) (PEOT/PBT). These factors, along with the gravity force, contribute to fast cell sedimentation toward the scaffold's bottom and mediocre attachment to the scaffold's filaments upon conventional static seeding, which is a simple and widely used seeding method that consists of placing a droplet of cell suspension on the top of the scaffold surface that gradually flows into the scaffold's pores.[5−7]

Different strategies have been considered to optimize cell attachment during static seeding of 3D ME-AM. For instance, loading cells into a natural or synthetic hydrogel solution, which cross-links within the scaffold pores, has shown to improve cell retention within the scaffold.[8,9] Alternatively, we

Received: November 3, 2020
Accepted: December 30, 2020

© XXXX The Authors. Published by American Chemical Society

have recently proposed the use of macromolecules as temporary seeding media supplements to increase its viscosity or density, which has proven to reduce cell sedimentation velocity and result in homogeneous cell attachment along the scaffold's cross-section.[4] Besides the modification of the seeding solution, the alteration of the scaffold architecture, with regard to pore size, lay-down pattern, or the introduction of vertical gradients, has also been suggested to enhance cell attachment.[6,10] Furthermore, synthetic polymers have been blended with bioactive fillers, such as calcium phosphates,[11] bioactive glass,[12] or graphene derivatives,[13] to improve cell attachment and cell−material interactions by increasing scaffolds' hydrophilicity and/or surface roughness.

Surface coatings have also been considered as an alternative to increase polymeric scaffolds' bioactivity, as some of the methods described above involve the modification of scaffold geometry or the material bulk properties and these can negatively affect the scaffold's mechanical properties. For example, NaOH etching or other wet chemical surface modifications can increase the hydrophilicity and surface roughness or deposit specific monomers with functional groups on 3D scaffolds.[14] However, the use of harsh chemicals can potentially compromise the integrity of the scaffolds' structure.[15] Other examples exploit scaffold's filament coatings with extracellular matrix (ECM) proteins or cell-adhesive peptides to improve cell adhesion.[16] Nevertheless, this approach has not been extensively explored due to proteins' limited half-lives and high costs.

Non-thermal plasma (NTP) surface modification has the advantage of altering the polymer surface chemistry and/or topography without the use of solvents while maintaining their bulk properties.[17] Various types of gases, such as oxygen, helium, argon, nitrogen, or their combination, can be used to generate the plasma discharge and activate polymer surfaces by the incorporation of hydroxyl, carboxyl, aldehyde, or amine groups. To obtain more stable coatings with a higher density of functional groups, the plasma discharge can be fed with monomers, such as alkyl amine or ammonia, or acrylic acid, to coat the surface with a thin polymeric film-containing amine or carboxyl groups, respectively, in a process known as plasma polymerization. NTP is an established technique to treat two-dimensional (2D) polymeric surfaces, where extensive research has revealed enhanced protein adsorption and cell attachment due to the presence of functional groups compared to methyl only containing surfaces.[18,19] Moreover, carboxyl-modified surfaces have shown to promote chondrogenesis, while amine groups have proved to direct cells toward the osteogenic pathway.[20−22]

NTP has been used during the last decade to functionalize 3D ME-AM scaffolds as well. Oxygen plasma activation, as one of the primary focuses of reported studies, has shown to increase surface roughness, protein adsorption, and cell attachment, as well as to promote alkaline phosphatase (ALP) expression and matrix mineralization on PCL scaffolds.[23,24] Other studies have explored plasma polymerization techniques. Among these, nitrogen-containing groups have been introduced on PCL or polystyrene scaffolds by allylamine, ammonia, or ethylene/N_2, promoting Runt-related transcription factor 2 (RUNX2) and ALP upregulation in human mesenchymal stromal cells (hMSCs) compared to untreated scaffolds.[25,26] Alternatively, in a study using PEOT/PBT scaffolds treated with acrylic acid plasma polymerization, enhanced proliferation and glycosaminoglycan production by chondrocytes were shown.[27] Despite promising results in enhancing ME-AM scaffold surface bioactivity, NTP is still not a widely used technique for 3D scaffold treatment. This is mainly due to the NTP process usually being carried out at subatmospheric pressures, where plasma has been shown to not ignite inside the scaffold pores.[28,29] This limits the treatment in the scaffold's core to diffusion, leading to inhomogeneous and uncontrolled gradient functionalization. Moreover, the process often requires costly vacuum equipment and its application demands multistep processes. Overcoming these limitations, atmospheric pressure plasma jets (APPJ) have been developed,[30] where the need for a reactor chamber and vacuum equipment is eliminated and the NTP exiting the jet can be directed into the scaffold pores or a region of interest. Moreover, APPJ enables its assembly to an AM platform, where the printing and plasma treatment processes can take place in a single hybrid system. This allows to plasma treat the scaffolds as a whole from the top, in a layer-by-layer manner to reach deep pores in large anatomical scaffolds, or zonally at specific scaffolds' regions.[31,32]

Taking these advantages, here we used a hybrid AM technique consisting of a ME printhead and an APPJ module assembled on a three-axis platform to fabricate plasma-treated PEOT/PBT scaffolds in a single process.[32] Despite its excellent processability and previous in vitro and in vivo applications for bone tissue engineering, PEOT/PBT demonstrates poor cell attachment upon cell seeding.[4,7] The organosilane monomers (3-aminopropyl)trimethoxysilane (APTMS) and maleic anhydride-vinyltrimethoxysilane (MA-VTMOS) were used to deposit polymer-like thin films containing amine and carboxyl functional groups, respectively, by plasma polymerization in argon on the PEOT/PBT scaffold surface. Despite being already explored to modify 2D surfaces,[33,34] these monomers were used here for the first time to treat 3D scaffolds. Compared to other precursors, organosilanes possess the advantage of providing a stable siloxane backbone to the coating, which is highly adherent and resistant to delamination in water conditions, ensuring good functional group retention under cell culture conditions.[35,36] Pristine scaffolds, plasma-polymerized scaffolds, and argon plasma-activated scaffolds were seeded with hMSCs. The cell attachment and adhesion mechanism were evaluated. Moreover, proliferation and osteogenic differentiation were assessed and compared among the different plasma conditions.

2. MATERIALS AND METHODS

2.1. Plasma-Treated Scaffold Fabrication and Characterization. Scaffolds were fabricated and plasma treated with a hybrid AM platform, consisting of a 3D axis stage (BioScaffolder 3.0, Gesim) equipped with a custom-made ME printhead and an APPJ (Plasma Stylus Noble, Nadir srl),[37] all enclosed in a poly(methyl methacrylate) box with fume extraction ventilation. In the first step, scaffolds were produced (Figure S1A). For that, PEOT/PBT pellets (300PEOT55PBT45, poly(ethylene oxide) (PEO) molecular weight = 300 kDa, PEOT:PBT weight ratio = 55:45, intrinsic viscosity 0.51 dL/g, PolyVation, The Netherlands) were heated up to 195 °C in the cartridge of the printhead. The molten polymer was extruded through a 250 μm internal diameter needle (pressure 7 bar, translation speed of 16 mm/s), depositing a 0−90 pattern block (15 × 15 × 4 mm^3) with a 200 μm layer thickness and a 750 μm strand distance (center to center) (Figure S1A).

Right after fabrication, scaffolds were plasma treated with the APPJ (Figure S1B). The device is based on a dielectric barrier discharge scheme simultaneously powered by a high-voltage (HV) generator (10 kV, 17 kHz) and a radio-frequency (RF) generator (27 MHz)

https://dx.doi.org/10.1021/acsami.0c19687
ACS Appl. Mater. Interfaces XXXX, XXX, XXX−XXX

(Figure S1C). Electrodes are positioned externally to an alumina duct where argon is fluxed (Ar 5.0 purity, 10 L/min) and plasma is ignited. An inner coaxial tube allows for the introduction of the precursors in the vapor phase just before the RF electrodes. For APTMS plasma polymerization, APTMS (Sigma-Aldrich) was carried into the plasma zone by argon gas passing through a bubbler at room temperature (RT) (flow = 2 L/min). Similarly, for MA-VTMOS plasma polymerization, MA (Sigma-Aldrich) and VTMOS (Sigma-Aldrich) in two independent bubblers were carried into the plasma zone by argon at 1.764 and 0.233 L/min, respectively. For argon activation, the RF generator was operated with a power output of 15 W in a continuous mode. For APTMS and MA-VTMOS plasma polymerization, the RF generator was operated in a pulsed mode, at a duty cycle of 5% (250 μs ON, 5000 μs OFF), with the power output for the ON duration set to 15 W. An outer gas shell of nitrogen (15 L/min) was used during the process to prevent precursor oxidation by the environmental air during the deposition. The APPJ nozzle was positioned at 1 mm above the scaffold surface and moved in *XY* following the surface filaments' path at 1 mm/s. For further studies, plasma-treated scaffolds were used within 2 days after plasma treatment ("fresh" samples) or after ~10 days being stored at RT in a sealed container ("aged" samples).

To assess the successful deposition of an APTMS plasma-polymerized layer, fresh, aged, and ethanol disinfected scaffolds were incubated with the amine-reactive fluorescent dye LIVE/DEAD fixable dead cell stain kit (Thermo Fisher Scientific) for 45 min at a concentration of 0.5/500 μL phosphate-buffered saline (PBS). Untreated, argon, and MA-VTMOS-treated scaffolds were also stained as controls. After PBS washes, scaffolds were cut and the cross-sections were imaged using a fluorescence microscope (Eclipse, Ti2-e, NIKON). To confirm the deposition of a MA-VTMOS layer, fresh, aged, and ethanol disinfected scaffolds were incubated for 20 s in a methylene blue solution (1 mg/mL). Untreated, argon, and APTMS-treated scaffolds were also stained as controls. After PBS washes, scaffolds were cut and imaged using a stereomicroscope (Nikon SMZ25). To evaluate the dynamic wettability of the scaffolds, a 35 μL water droplet was carefully deposited onto the surface of the scaffolds, and the wetting behavior was captured with a digital camera at 1 frame/s (Krüss DSA25S).

2.2. Plasma-Treated 2D Film Fabrication and Characterization. 2D films were prepared from PEOT/PBT pellets. Briefly, 60 mg of pellets were molten at 190 °C and pressed with a coverslip against a Teflon sheet to obtain films with a 14 mm diameter and ~300 μm thickness. Subsequently, PEOT/PBT films were plasma treated with argon, APTMS, or MA-VTMOS using the APPJ, according to the parameters in Section 2.1.

The static contact angle was measured in fresh and aged films using the sessile drop method. For that, a 4 μL water droplet was placed on top of the substrates by an automatic syringe dispenser (Krüss DSA25S). Twenty seconds after droplet formation, the contact angle was calculated automatically by device's software using the Laplace–Young curve fitting.

Attenuated total reflectance-Fourier-transform-infrared (ATR-FTIR) spectroscopy (Nicolet iS50, diamond ATR) was performed on untreated and fresh plasma treated films to further confirm the presence of the coating.

ζ potential measurements were performed on fresh films with a size of 2 × 4 cm^2. Electrokinetic measurements were performed at RT using a SurPASS system (Anton Paar GmbH, Germany), with a KCl solution (0.01 M, pH 5–5.5) as an electrolyte. The ζ potential was calculated from 10 experimental points taken by the measurement of the streaming potential in a pressure range of 500 mbar (start) to 200 mbar (end) in the flow cell.

2.3. Cell Seeding on 3D Scaffolds. HMSCs isolated from bone marrow were purchased from Texas A&M Health Science Center, College of Medicine, Institute for Regenerative Medicine. Cryopreserved vials were plated at a density of 1000 cells/cm^2 in tissue culture flasks and expanded at 37 °C/5% CO_2 in cell culture media (CM) consisting of α-minimum essential medium (αMEM) with Glutamax and no nucleosides (Gibco) supplemented with 10% fetal bovine serum (FBS).

To investigate the cell attachment mechanism, fresh scaffolds were disinfected in 70% ethanol for 20 min and washed three times with Dulbecco's PBS (5 min each). Scaffolds were incubated overnight in CM with FBS ((+)FBS) or CM without FBS ((−)FBS). Before seeding, scaffolds were dried on top of a sterile filter paper and placed on untreated well plates. HMSCs were trypsinized and resuspended in (+)FBS or (−)FBS CM. A droplet of cell suspension (37 μL containing 200 000 cells) was placed on top of each scaffold, filling the pores within some seconds. Seeded scaffolds were incubated for 4 h at 37 °C/5% CO_2 to allow for cell attachment. After this time, scaffolds were collected or transferred to new wells containing 1.5 mL of (+)FBS and cultured overnight before sample collection. Aged scaffolds incubated overnight in (+)FBS CM and seeded on (+)FBS CM were also cultured overnight before sample collection to analyze the effect of aging on cell adhesion.

To evaluate the effect of cell seeding density on scaffold coverage and proliferation, fresh and aged scaffolds were incubated overnight in CM and seeded with hMSCs in CM at a density of 200 000 (200k) or 400 000 (400k) cells/scaffold, concentrated in a 37 μL droplet. After 4 h attachment, 200k and 400k scaffolds were transferred to new wells containing 1.5 or 3 mL of BM (CM supplemented with 200 μM L-ascorbic acid 2-phosphate), respectively, and cultured for 7 days.

To evaluate hMSC osteogenic differentiation, aged plasma-treated scaffolds were incubated overnight in (+)FBS. Scaffolds seeded with 200 000 cells were further cultured for 7 days in BM and for another 47 days in mineralization media (MM) consisting of BM supplemented with dexamethasone (10 nM) (Sigma-Aldrich) and β-glycerophosphate (10 mM) (Sigma-Aldrich). Media was replaced every 2 or 3 days. As osteogenic differentiation 2D controls, the cells were seeded in tissue culture polystyrene well plates at a density of 5000 cells/cm^2 and cultured in the same media conditions as 3D scaffolds.

2.4. Imaging of Cell Attachment within Scaffold Cross-Sections. Scaffolds were fixed with 4 wt % paraformaldehyde for 30 min, permeabilized using 0.1 vol % Triton-X for 30 min, and incubated with phalloidin (Alexa Fluor 488, 1:75 dilution in PBS) for 1 h at RT. The bottom and cross-section of scaffolds were imaged using a fluorescence microscope. Background subtraction and contrast enhancement were performed on the images using the software ImageJ to clarify their visualization. To assess cell coverage, cross-section images were converted to binary (rendering regions with cells in white and the rest in black), and the total amount of white pixels in the scaffold area was quantified and normalized to the total number of pixels.

2.5. DNA Quantification. The scaffolds collected at the desired time points were freeze-thawed 3× for cell lysis and incubated overnight at 56 °C in proteinase K solution (1 mg/mL proteinase K (Sigma-Aldrich) in Tris/ethylenediaminetetraacetic acid (EDTA) buffer) (1:1) for matrix degradation and cell lysis. Then, the scaffolds were freeze-thawed 3× and incubated 1 h at RT with a 20× diluted lysis buffer from the CyQUANT cell proliferation assay kit (Thermo Fisher Scientific) containing RNase A (1:500) to degrade cellular RNA. Finally, the samples were incubated with the fluorescent dye provided by the kit (1:1) for 15 min and fluorescence was measured using a spectrophotometer (emission/excitation = 520/480 nm) (CLARIOstar, BMG Labtech).

2.6. Protein Adsorption Quantification. Disinfected fresh and aged scaffolds were incubated overnight at 37 °C in (+)FBS or (−)FBS. After washing with PBS, scaffolds were blocked for 1 h at 37 °C in 1% w/v bovine serum albumin (BSA)/PBS and then incubated with specific bovine vitronectin (Vn) (ab23444, Abcam) or fibronectin (Fn) (ab2413, Abcam) primary antibodies, diluted 1:500 and 1:400, respectively, in 1% w/v BSA/PBS. After washing three times in PBS, scaffolds were incubated for 1 h at 37 °C in horseradish peroxidase (HRP)-conjugated anti-mouse secondary antibody (Abcam, 1:100 000 dilution 1% BSA) for Vn detection or HRP-conjugated anti-rabbit secondary antibody (Abcam, 1:10 000 dilution in 1% BSA) for Fn detection. After three washes in 1% BSA+

https://dx.doi.org/10.1021/acsami.0c19687
ACS Appl. Mater. Interfaces XXXX, XXX, XXX–XXX

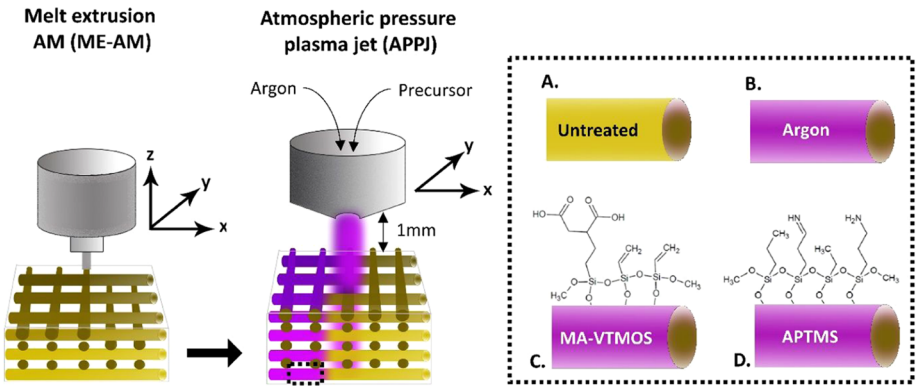

Figure 1. Schematic representation of the hybrid platform for scaffold fabrication combined with plasma functionalization. 3D scaffolds are fabricated via melt extrusion AM (ME-AM) and, consequently, plasma treated from the top using an atmospheric pressure plasma jet (APPJ), which moves in *XY* following the scaffold filaments while the plasma penetrates the scaffold depth. As a result, (a) untreated, (b) argon activated, or (c) MA-VTMOS and (d) APTMS plasma-polymerized scaffolds can be obtained, each with a specific surface functionality.

0.05% Tween 20, scaffolds were blotted in an adsorbent paper and incubated in 150 μL of 1-Step Ultra TMB ELISA substrate (Thermo Fisher Scientific). The color was allowed to develop for 10 min at RT, and the reaction stopped with 50 μL of sulfuric acid (2 M). Supernatant absorbance was measured at 450 nm using a spectrophotometer. Scaffolds that were incubated in (−)FBS and (+)FBS and reacted with only secondary antibodies were used as controls.

To analyze albumin adsorption, disinfected fresh and aged scaffolds were incubated overnight at 37 °C with 1 mg/mL of BSA−fluorescein isothiocyanate (FITC) (Sigma-Aldrich) solution in PBS. After washing three times with PBS, scaffolds were blotted in an adsorbent paper and incubated for 2 h at RT in a 1% sodium dodecyl sulfate (SDS) solution. Supernatant fluorescence was measured at excitation/emission = 495/519 nm.

2.7. Alizarin Red S (ARS) Staining. Scaffolds were collected at 35 and 54 days of culture, fixed, washed with distilled water, cut into half, and stained with ARS (60 mM, pH 4.1−4.3) for 20 min at RT. The samples were thoroughly washed to remove staining residues. Scaffolds' cross-sections were imaged using a stereomicroscope to visualize calcium deposition.

2.8. Immunostaining. After fixation, scaffolds were permeabilized for 30 min by incubating on Triton-X 100 (0.1 vol %). Subsequently, scaffolds were blocked by 1 h incubation in blocking buffer (BB, 3% BSA + 0.01% Triton-X 100), cut into half, and incubated overnight at 4 °C with a primary antibody: either collagen I rabbit polyclonal (ab34710, Abcam) or vinculin mouse monoclonal (sc73264, Santa Cruz Biotechnology), both diluted 1:200 in washing buffer (WW, 10× diluted blocking buffer). Washed samples were incubated for 1 h at RT with the secondary antibody (1:200 in WW, Alexa Fluor 568 goat derived anti-rabbit antibody, Thermo Fisher Scientific). Then, the scaffolds were washed and stained for F-actin (1:200 dilution in PBS, 488 Alexa Fluor Phalloidin, Thermo Fisher Scientific) for 1 h at RT and imaged using a confocal laser scanning microscope (Leica TCS SP8 STED), equipped with a white light laser (WLL). Emission was detected with HyD detectors.

2.9. Gene Expression. Gene expression was analyzed with the quantitative reverse transcription polymerase chain reaction (qRT-PCR) at 14 and 54 days of culture. RNA was extracted from the cells by incubating the scaffolds in Trizol. Subsequently, samples were centrifuged at 12 000 rcf for 5 min to precipitate the scaffold and ECM at the bottom. In the last step, chloroform was added to the supernatant and centrifuged at 12 000 rcf for 5 min to isolate the RNA present in the aqueous phase. RNA was further purified using the RNeasy mini kit column (Qiagen) according to the manufacturer's protocol and quantified using a spectrophotometer. Reverse transcription was performed using iScript (Bio-Rad) following the suppliers' protocol. Quantitative polymerase chain reaction (qPCR) was performed on the mix composed of cDNA, SYBRGreen master mix (Qiagen), and the selected primers (Table S1) using a CFX Connect real-time system (Bio-Rad) under the following conditions: cDNA denaturation for 3 min at 95 °C, 40 cycles of 15 s at 95 °C, and 30 s at 65 °C. Gene transcription was normalized to the transcription of the housekeeping gene β-2-microglobulin (B2M). The $2^{-\Delta\Delta Ct}$ method was used to calculate relative gene expression for each target gene.

2.10. Statistical Analysis. All data are shown as average with error bars indicating the standard deviation (s.d.) of at least three replicates. Analysis of statistics was conducted with GraphPad software. A one-way or two-way analysis of variance (ANOVA) was performed with Tukey's post hoc multiple comparison test to evaluate statistical significance.

3. RESULTS AND DISCUSSION

Compared to conventional manufacturing techniques, the possibility of fabricating customizable scaffolds for bone tissue engineering in a reproducible manner by AM brings the produced constructs one step closer to clinical translation. The assembly of a surface modification module, such as an APPJ, into the printing platform further increases the value of the technology and fabricated scaffolds for their research and clinical applications. With such a hybrid AM platform developed within our groups,[32] we were able to manufacture surface-modified 3D PEOT/PBT scaffolds in a continuous process, where scaffolds are fabricated by ME-AM and subsequently functionalized by the APPJ module (Figure 1). To do this, the nozzle tip of the APPJ module was adjusted at 1 mm over the scaffold surface, ensuring the penetration of the plasma flame over the whole scaffold depth (4 mm) while moved in *XY* over the scaffold filaments at the transitional speed of 1 mm/s, covering the whole scaffold block area (15 × 15 mm^2).

3.1. Plasma Scaffold Characterization. Plasma polymerization of APTMS and MA-VTMOS on the surface of the scaffolds was carried out in a pulsing mode with a 5% duty cycle because compared to continuous plasma, pulsed plasma polymerization at low duty cycles has shown to allow for better preservation of the monomers' functional groups integrity during radical formation, as well as for the deposition of smoother surfaces.[33,36,38] A homogeneous negatively charged coating covering the filaments all along the scaffold volume after MA-VTMOS plasma polymerization was confirmed by staining with the cationic dye methylene blue, as previously described (Figures 2A and S2), as well as with ζ potential

https://dx.doi.org/10.1021/acsami.0c19687
ACS Appl. Mater. Interfaces XXXX, XXX, XXX−XXX

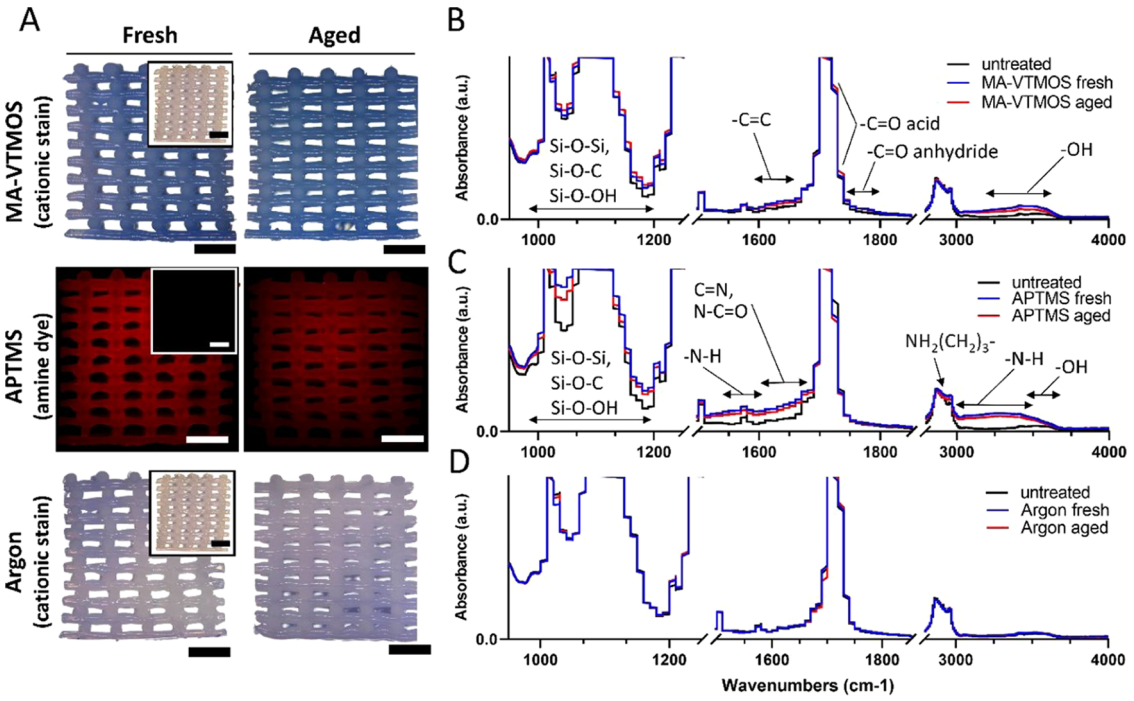

Figure 2. Characterization of plasma-functionalized 3D scaffolds and comparison among fresh and aged conditions. (A) Verification of the treated scaffold surface functionalization by specific staining. MA-VTMOS and argon treated scaffolds were stained with the cationic dye methylene blue (blue staining in light microscopy) and APTMS treated scaffolds with an amine-specific dye (red staining in fluorescence microscopy). Insets represent stained untreated PEOT/PBT control scaffolds (white in light microscopy and gray in fluorescence microscopy). Scale bars 1 mm. (B–D) FTIR spectra of MA-VTMOS, APTMS, and argon plasma-treated 2D substrates (melt-pressed PEOT/PBT films).

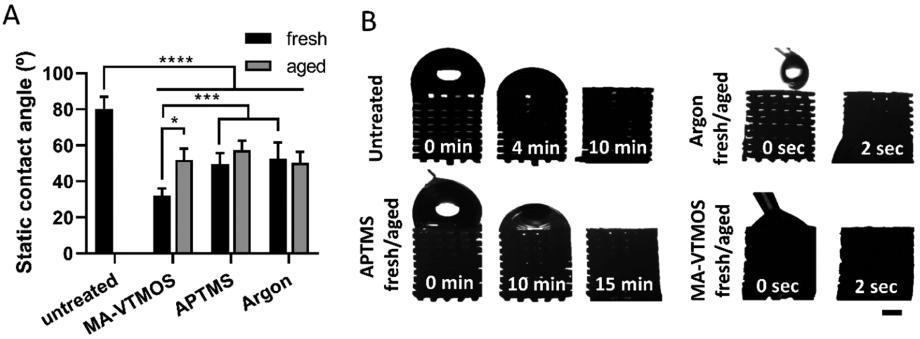

Figure 3. Hydrophilicity and wettability of plasma-functionalized 3D scaffolds and comparison among fresh and aged conditions. (A) Static contact angle measured on untreated and plasma-treated 2D substrates. Data presented as average ± s.d. and statistical significance performed using two-way ANOVA with Tukey's multiple comparison test (*p < 0.05, ***p < 0.001, ****p < 0.0001). (B) Dynamic wettability of plasma-treated scaffolds. Scale bar 1 mm.

measurements (Figure S3).[39] FTIR analysis further identified the negatively charged functional groups as intact anhydride groups (−C═O stretching at 1750−1800 cm^{-1}) and carboxyl groups (−OH stretching at 3200−3650 cm^{-1}) from the MA precursor (Figures 2B and S4A).[38,40] In addition, vinyl groups from the VTMOS molecules (C═C stretching at 1630−1660 cm^{-1}) were also identified. To visualize the formation of a homogeneous positively charged (Figure S3) thin polymer-like film containing amine groups ($-NH_2$) after APTMS plasma functionalization, an amine-reactive fluorescent dye was used to stain the scaffolds (Figures 2A and S2). Primary amine vibrations were also observed by FTIR analysis (N−H bending at 1560−1630 cm^{-1} and N−H stretching at 3000−3500 cm^{-1}) (Figures 2C and S4B). Stretching vibrations visible at 2980−2880 cm^{-1} confirmed the retention of some aminopropyl chains of the precursor.[41] Nitrogen-containing groups were also visible as amides (−C═O stretching at 1630−1695 cm^{-1}) and oximes (C═N stretching at 1650−1680 cm^{-1} and O−H stretching at 3550−3600 cm^{-1}).[42,43] The presence of oximes and amides was probably due to precursor oxidation during the deposition process, despite the nitrogen being flushed in the outer duct of the APPJ, probably due to the jet movement and the flow being disrupted by the scaffold structure.[41] In addition, the APTMS and MA-VTMOS plasma-polymerized substrate spectra were dominated by absorption bands between 1000 and 1200 cm^{-1}, confirming the presence of a siloxane network. In contrast to plasma polymerization, argon plasma activation is a less specific treatment, where a variety of polar groups can be introduced. According to previous reports on argon plasma on PEOT/PBT substrates, it is hypothesized that hydroperoxide (−OOH) and peroxide (−OO−) groups were incorporated, formed after postoxidation in air of the free

https://dx.doi.org/10.1021/acsami.0c19687
ACS Appl. Mater. Interfaces XXXX, XXX, XXX−XXX

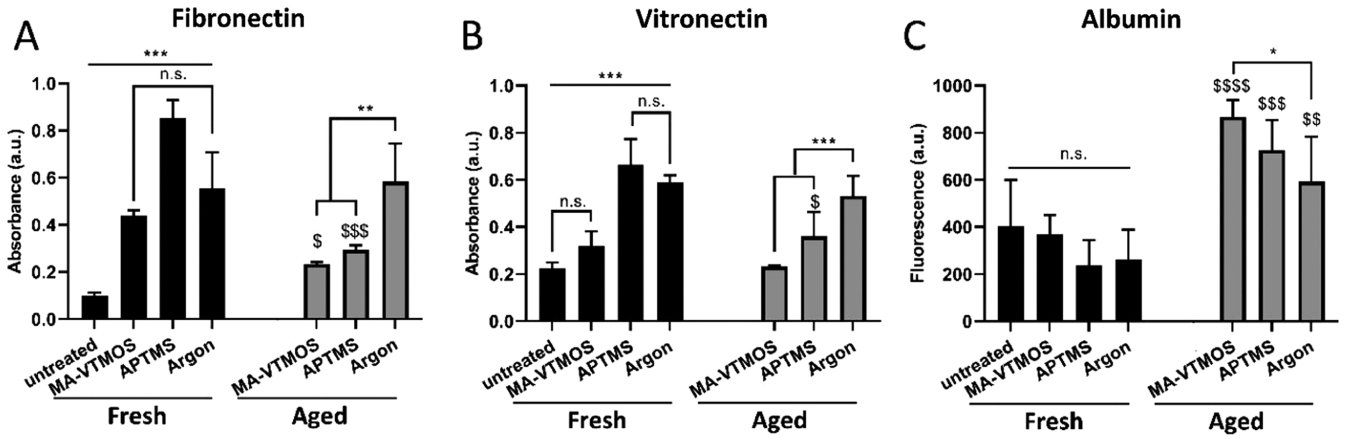

Figure 4. Protein adsorption to scaffolds upon incubation in serum-containing medium ((+)FBS): effect of plasma functionalization and aging conditions. Relative amounts of adsorbed (A) fibronectin, (B) vitronectin, and (C) albumin to untreated scaffolds and fresh and aged MA-VTMOS, APTMS, and argon plasma-treated scaffolds. Data presented as average ± s.d. and statistical significance performed using two-way ANOVA with Tukey's multiple comparison test (n.s., $p > 0.05$, $^{*\$}p < 0.05$, $^{**\$\$}p < 0.01$, $^{***\$\$\$}p < 0.0001$; * for comparisons among treatments within aged or fresh scaffolds; $ for comparisons among fresh and aged for each plasma treatment).

radicals generated by plasma, along with aldehyde or ketone groups (−CHO, −CO−).[44−46] The presence of these negatively charged groups exposed to the surface of the scaffolds was visualized by a low-intensity methylene blue staining and confirmed by ζ potential measurements (Figures 2A and S3). However, these changes were not detected by FTIR analysis, possibly due to the very subtle variation in surface chemistry (Figures 2D and S4C). In addition, it is plausible that argon plasma activation could have induced changes in the surface roughness of PEOT/PBT, as previously described.[46] This effect has been attributed to plasma UV irradiation etching, mainly on the PEO amorphous regions of the copolymer, which are more mobile and susceptible to plasma than the PBT regions. However, scanning electron microscopy (SEM) image analysis did not show any changes in the microscale surface roughness of argon scaffolds compared to untreated ones (Figure S5). Similarly, no changes in microroughness were noted on the plasma-polymerized scaffolds (Figure S5). This might be due to the low contact time of the plasma jet with the polymer (some seconds), compared to the long exposure-driven changes reported in the literature (5−30 min),[44,45] modifying only the roughness in the nanoscale, which was not appreciable with SEM.

To evaluate the effect of plasma treatment on the polymer wettability, water contact angle (WCA) measurements were performed on melt-pressed PEOT/PBT films, where enhanced hydrophilicity was observed due to the introduction of polar groups by all of the plasma conditions (Figure 3A). WCA decreased from ∼80° to ∼55° in argon and APTMS-treated scaffolds, and down to ∼35° in MA-VTMOS scaffolds. Interestingly, similar values were previously reported for self-assembled monolayers coated with these specific functional groups.[47] In accordance with the WCA, the dynamic wettability of MA-VTMOS and argon-treated scaffolds increased compared to untreated scaffolds. This was observed by a significant reduction in the time that a droplet of water placed on top of the scaffold took to fill the scaffold pores (from 6 min on untreated scaffolds to 2 s on treated scaffolds), mimicking the static seeding process (Figure 3B). Surprisingly, despite the low contact angle of the APTMS coatings, the wettability of these scaffolds decreased compared to untreated scaffolds, potentially due to the lower density of functional groups and higher density of hydrophobic silane/siloxane in the scaffolds compared to the 2D films, where the WCA was measured. However, this did not affect cell culture experiments since scaffolds were always prewetted before cell seeding.

The effect of storage (∼10 days at RT in a sealed container) on the preservation of the plasma activation or polymerized treatments was also evaluated. This is a relevant shelf-life information due to the potential time-lapse between the scaffold production and its use, both for in vitro and in vivo applications. It is well know that plasma-treated polymeric surfaces can undergo aging over time, which accounts for surface restructuring and hydrophobicity recovery toward a more energetically stable state.[48] While bulk analysis in terms of staining intensity, contact angle values, and wettability suggested stability of the coatings (Figures 2A and 3A,B), FTIR analysis revealed slightly lower functional group absorbance peaks on aged substrates compared to fresh ones (Figure 2B−D), as previously reported for such plasma treatments on 2D substrates.[40,49] Moreover, it is worth noticing that the carbonyl stretching absorbance in MA-VTMOS spectra (−C═O stretching at 1700−1725 cm^{-1}) slightly increased in aged samples, which can be explained by the formation of carboxylic groups by the hydrolysis of the anhydrides through humidity.[40] It is possible that the semi-crystalline property of PEOT/PBT and the particularly efficient but cold and homogeneous APPJ configuration might have contributed to the limited aging effect, since it has previously been shown that the hydrophobic recovery decreases with increasing polymer crystallinity and with decreasing degree of cross-linking due to plasma jet surface interaction.[50−52] In general, these results suggest small changes in surface chemistry given by a reduction in the functional group density on aged plasma-polymerized substrates, which could potentially influence interactions such as protein adsorption or cell attachment.

3.2. Protein Adsorption. The effect of plasma treatment type and aging on protein adsorption after scaffold incubation in cell culture media containing serum ((+)FBS) was analyzed (Figure 4). It was observed that fibronectin (Fn) and vitronectin (Vn), two relevant cell-adhesive proteins present in serum, adsorbed in greater amounts to fresh plasma-treated scaffolds than to untreated scaffolds (Figure 4A,B). Upon

https://dx.doi.org/10.1021/acsami.0c19687
ACS Appl. Mater. Interfaces XXXX, XXX, XXX−XXX

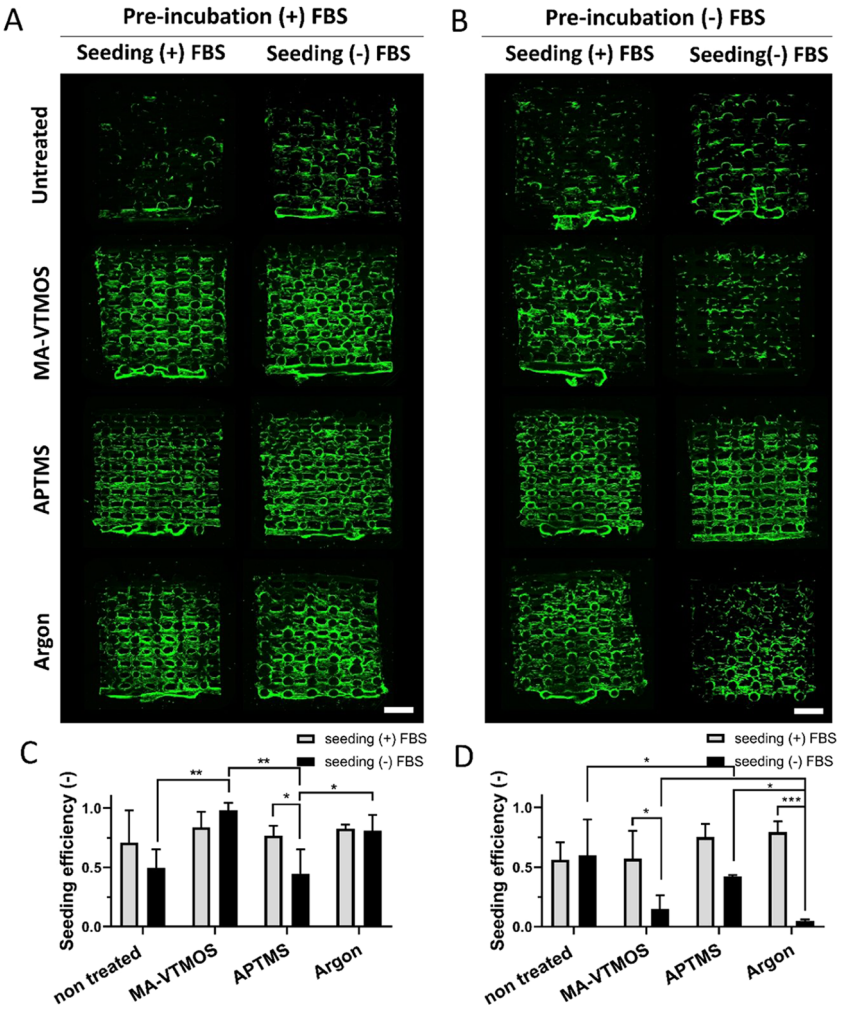

Figure 5. Cell coverage and cell seeding efficiency on fresh plasma-treated scaffolds under different preincubation and seeding conditions. Fluorescence microscopy images (F-actin, green) of hMSCs in the cross-sections of scaffolds after 24 h of culture, and (A) preincubated with (+)FBS or (B) (−)FBS, and seeded with (+)FBS or (−)FBS. Quantification of cell seeding efficiency on scaffolds (C) preincubated with (+)FBS and (D) preincubated with (−)FBS. Data presented as average ± s.d. and statistical significance performed using two-way ANOVA with Tukey's multiple comparison test (*$p < 0.05$; **$p < 0.01$; ***$p < 0.001$). Scale bars 1 mm.

(+)FBS incubation, albumin, which is present at 100−1000 times higher concentration than adhesion-promoting proteins, adsorbs in the early phase of the protein layer formation. It is hypothesized that the hydrophobic interactions of albumin with the untreated PEOT/PBT are strong and resistant to displacement by Fn and Vn, while these proteins can effectively displace the weakly adsorbed albumin on the hydrophilic and charged plasma-treated surfaces.[53,54] Notably, the adsorption of Fn and Vn was significantly higher on APTMS scaffolds, which can be attributed to the electrostatic interactions between the positively charged amine-based scaffolds' surface and the negatively charged proteins in solution, leading to high protein adsorption (Figure 4A,B). However, the theory of electrostatic interactions cannot explain the high adsorption of negatively charged Fn and Vn to the negative charge of the surface of MA-VTMOS and argon scaffolds, compared to untreated scaffolds. Previous studies have also shown that Fn can be adsorbed at similar rates and amounts to both hydrophilic positively charged and negatively charged surfaces with ζ potential values similar to those measured within this study.[55] This has been explained by charged microdomains of the proteins yielding short-range attractions, which can lead to hydrogen bond formation once the Debye interactions overcome the macroscopic electrostatic repulsions. Alternatively, adsorption of Fn or Vn to negatively charged polymers has been explained by the first adsorbed layer of positively charged serum proteins, such as laminin, allowing subsequent electrostatic interactions with the negatively charged proteins.[56] Interestingly, the reduction in functional group density and, potentially, surface charge caused by aging led to a significant reduction in Fn and Vn adsorption and a significant increase in albumin adsorption (Figure 4C) to MA-VTMOS and APTMS aged scaffolds. This resulted in comparable Fn and Vn adsorption to both scaffold types, regardless of their surface charge. Notably, argon scaffolds were not affected in this regard by aging and presented the largest relative cell-adhesive protein adsorption values among aged plasma treatment types. This observation further strengthens the hypothesis that argon plasma activation mostly led to a surface roughness change, rather than to a chemical change; it is the nanoroughness, which remains unaltered over time, the feature responsible for cell-adhesive protein adsorption.[57]

3.3. Cell Adhesion Mechanism to Plasma-Treated Scaffolds. Enhanced cell attachment on 2D surfaces and 3D

https://dx.doi.org/10.1021/acsami.0c19687
ACS Appl. Mater. Interfaces XXXX, XXX, XXX−XXX

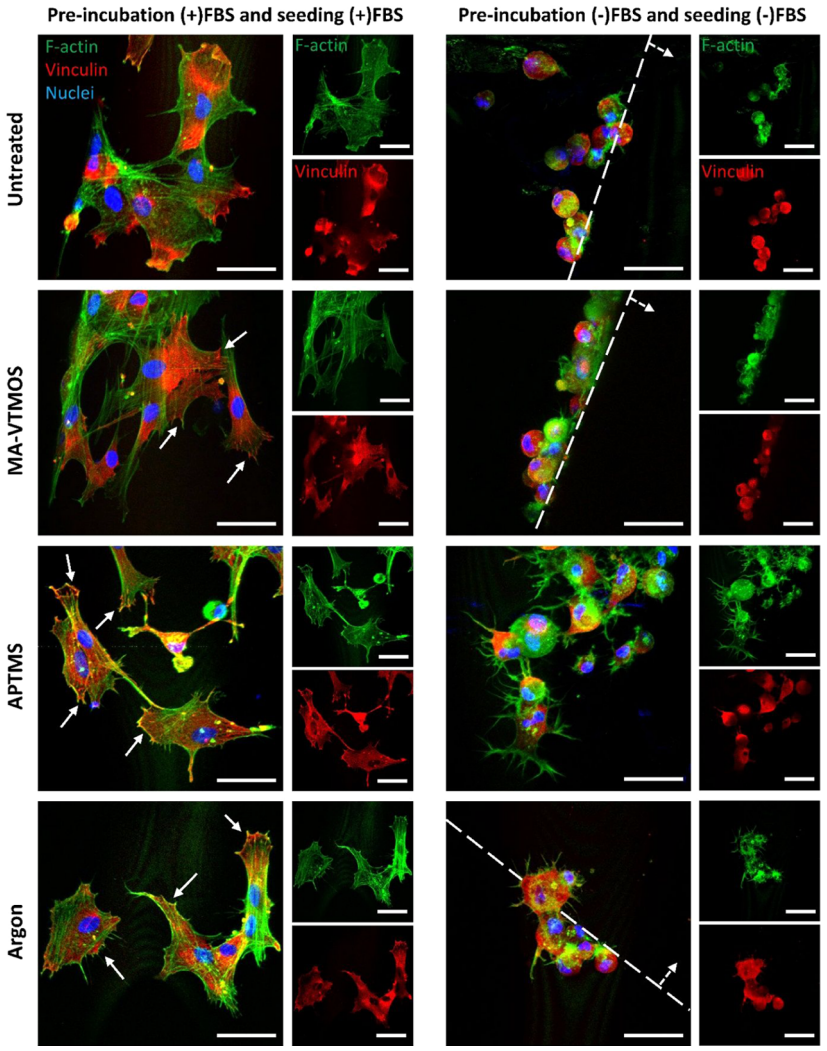

Figure 6. HMSC morphology and focal adhesion formation after 4 h seeding on fresh plasma-treated scaffolds preincubated and seeded in (+)FBS or (−)FBS. Representative confocal microscopy images of hMSCs (F-actin, green; nuclei, blue; vinculin, red) on top of scaffold filaments 4 h post-seeding. Continuous arrows indicate focal adhesions. Dashed lines delimitate the scaffold filament, with dashed arrows indicating the filament's surface. Scale bars 50 μm.

scaffolds containing polar functional groups has been attributed to surface wettability,[58] surface charge potential,[55,59] or amount of protein adsorption.[19] However, most of these studies have been performed in serum-containing media or in protein-coated surfaces, masking the potential effect of direct cell interactions with the functional groups and, therefore, not fully characterizing the mechanism of cell adhesion to specific surface chemistry. Thus, to discern among attachment mediated by electrostatic interactions with the charged surfaces and attachment via integrin binding to proteins adsorbed from serum, fresh scaffolds were preincubated for 24 h in (+)FBS or serum-free medium ((−)FBS), and subsequently seeded with hMSCs for 4 h in (+)FBS or (−)FBS. Representative fluorescence images of hMSCs on scaffolds' cross-section after overnight culture suggested an increase in cell attachment on plasma-activated and polymerized scaffolds, compared to untreated scaffolds, when these were preincubated in (+)FBS, regardless of the presence or absence of serum during the 4 h seeding (Figure 5A). This can be attributed to the higher adsorption of cell-adhesive proteins (Fn and Vn) to these scaffolds, as shown in Figure 4. Despite improving cell adhesion and distribution, cell sedimentation toward the bottom of the scaffold was observed both on untreated and treated scaffolds (Figure S6A). It is known that, regardless of the scaffold surface properties, the cells in the macropores, which are far from the scaffold filaments during the seeding process, are unable to interact with the scaffold's surface, leading to sedimentation toward the bottom and a monolayer formation. Looking at the quantitative values on seeding efficiency presented in Figure 5C, no differences in total cell attachment among scaffold types were observed when preincubated and seeded in (+)FBS. In turn, slightly higher cell attachment was noted on MA-VTMOS and argon scaffolds compared to APTMS and untreated scaffolds when preincubated in (+)FBS, but seeded in (−)FBS. In the case of APTMS, since cell distribution images show homogenous cell attachment in the cross-section comparable to other plasma conditions and to its (+)FBS seeding counterpart, it is plausible that lower cell adhesion on the bottom of the scaffold might have contributed to lower overall cell adhesion values. On the other hand, the sedimented cells that attached to the bottom of the untreated scaffolds might have significantly contributed to the relatively higher seeding efficiency values than expected for the low cell coverage on

https://dx.doi.org/10.1021/acsami.0c19687
ACS Appl. Mater. Interfaces XXXX, XXX, XXX−XXX

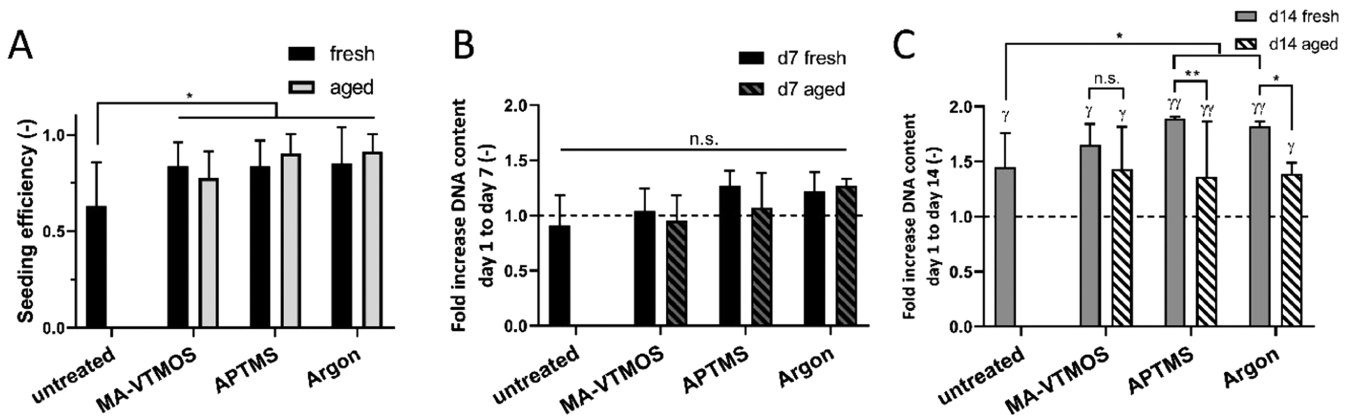

Figure 7. Effect of plasma treatment and aging conditions on cell seeding efficiency and proliferation. (A) Cell seeding efficiency and fold increase in the DNA content after (B) 7 days of culture (in BM), and (C) 14 days of culture (7 days in BM and 7 days in MM) with respect to day 1, which is marked with a dashed line. Scaffolds were preincubated and seeded with (+)FBS. Data presented as average ± s.d. and statistical significance performed using two-way ANOVA with Tukey's multiple comparison test (n.s. $p > 0.05$, $^{*\gamma}p < 0.05$, $^{**\gamma\gamma}p < 0.01$; * for comparisons among plasma treatments within aged or fresh scaffolds, and among fresh and aged scaffolds for each plasma treatment; γ for comparisons between the given time point and day 1 for each plasma treatment).

their cross-section. Interestingly, despite being preincubated in (−)FBS, homogeneous cell attachment was observed along the cross-section of plasma-treated scaffolds seeded in (+)FBS (Figure 5B), but not in untreated scaffolds. Furthermore, cell seeding efficiency values were comparable to those of scaffolds preincubated and seeded in (+)FBS (Figure S6C). These observations suggested that preincubation in (+)FBS was not necessary when the seeding process was performed in (+)FBS, regardless of the plasma treatment. This is likely due to protein adsorption, reaching an equilibrium already in short incubation times. In fact, serum proteins have been shown to adsorb to surfaces containing polar functional groups within the first minutes of incubation.[53,55] On the other hand, seeding with (+)FBS was necessary for optimum cell attachment on MA-VTMOS and argon scaffolds when preincubated in (−)FBS. In this case, seeding with (−)FBS on MA-VTMOS-treated scaffolds led to poor and comparable cell coverage in scaffold's cross-section to untreated scaffolds (Figure 5B), which together with the lack of sedimented cell layer formation on the bottom (cells remained on the well plate) contributed to significantly lower seeding efficiency (Figures 5D and S6B). Similarly, lower cell coverage and the absence of a cell monolayer at the bottom were observed in the cross-section of argon-treated scaffolds preincubated and seeded in (−)FBS, compared to other preincubation and seeding conditions. In both cases, due to the lack of protein attachment sites, the monolayer preferentially attached to the bottom of the seeding well plate rather than to the scaffold. Surprisingly, APTMS scaffolds preincubated and seeded in (−)FBS demonstrated a homogeneous and confluent cell coverage in the cross-section, as well as seeding efficiency values comparable to other preincubation and seeding conditions (Figures 5D and S6D). Overall, these results suggest that (i) MA-VTMOS plasma polymerization support cell attachment to scaffolds mostly through cell−protein interactions, and (ii) cell attachment on APTMS plasma-polymerized scaffolds is driven by cell−protein interactions in the presence of serum, and by electrostatic interactions between the cell and the amine groups coating the scaffold filaments in the absence of serum. The latter conclusion is in agreement with the previously published reports studying cell adhesion on 2D surfaces, suggesting that in protein-free conditions direct interactions between the negatively charged chondroitin sulfate proteoglycans in the cell membrane and the positively charged amine groups on a surface are responsible for promoting cell attachment.[58,60] On the other hand, repulsive electrostatic interactions between the negatively charged groups on the MA-VTMOS scaffolds and the cells do not allow for cell attachment in serum-free conditions. In the case of argon plasma treatment, we hypothesize that the nanoroughness itself[61] or combined with the lower presence of charged hydrophilic groups might have favored a slightly higher cell attachment in these scaffolds in serum-free conditions compared to MA-VTMOS-treated scaffolds.

To further analyze the cell attachment mechanism to the different plasma-treated scaffolds, cell morphology and focal adhesion formation in the absence or presence of serum were studied (Figure 6). Preincubation and seeding in (+)FBS led to cell spreading and the formation of F-actin stress fibers on hMSCs adhered to both untreated and plasma-treated scaffolds, only after the 4 h seeding. Moreover, while hMSCs did not show well-defined vinculin structures on untreated scaffolds, established focal adhesions at the end of the stress fibers in the periphery of the cells were visualized on the plasma-treated scaffolds, which was correlated to the higher amount of cell-adhesive proteins adsorbed on these surfaces, allowing for integrin binding (Figure 6). Larger vinculin expression, as well as increased focal adhesion kinase expression, which localizes to focal adhesions to activate migration, proliferation, and differentiation pathways, was also previously reported on amine-, carboxyl-, hydroxyl-, and argon-functionalized surfaces preincubated in Fn[20] or (+)FBS medium[62,63] compared to untreated surfaces. On the contrary, the few attached hMSCs to the untreated, MA-VTMOS and argon scaffolds showed a well-defined round morphology and lacked focal adhesion complexes when preincubated and seeded in (−)FBS, due to the repulsive electrostatic forces and the lack of cell-adhesive proteins hindering cell attachment spreading (Figure 6). The fact that, when looking at the scaffold cross-section, these cells were only found on the top surface of the filaments, further suggests that the cells passively laid on top of the filament due to gravity during the seeding process and that not active attachment occurred. On the contrary, hMSCs on APTMS scaffolds preincubated and

https://dx.doi.org/10.1021/acsami.0c19687
ACS Appl. Mater. Interfaces XXXX, XXX, XXX−XXX

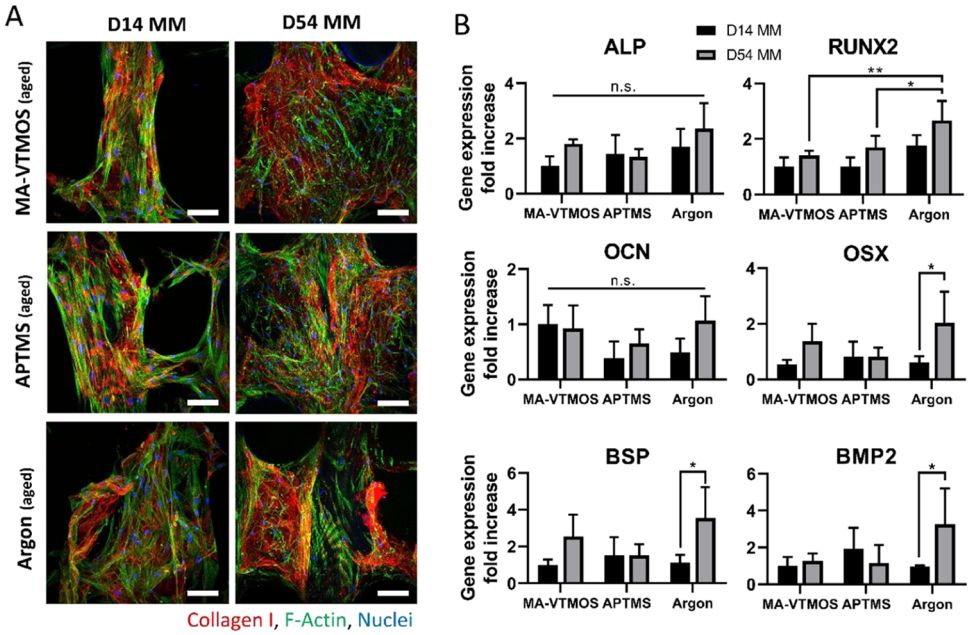

Figure 8. Evaluation of the osteogenic differentiation potential of hMSCs seeded on aged plasma-treated scaffolds. (A) Representative confocal microscopy images of hMSCs (F-actin, green) on top of scaffold filaments after 14 and 54 days of culture (7 and 47 days in MM, respectively) and stained for the relevant osteogenic marker COL1 (red). Scale bars 100 μm. (B) Gene expression of hMSCs after 14 and 54 days of culture (7 and 47 days in MM, respectively) comparing the three different plasma treatments. ALP, RUNX2, OCN, OSX, BSP, and BMP2 fold-change expression values relative to MA-VTMOS day 14. Data presented as average ± s.d. and statistical significance performed using two-way ANOVA with Tukey's multiple comparison test (n.s. $p > 0.05$; *$p < 0.05$; **$p < 0.01$).

seeded in (−)FBS were observed occupying the whole filament surface area. Interestingly, these cells were able to form multiple protrusions and F-actin fibers, which were not colocalized with focal adhesions, suggesting cell adhesion to the positively charged scaffold surface without mediation of integrin binding sites (Figure 6). Similar microfilament bundle formation and lack of focal contact formation were previously reported on fibroblast adhesion to 2D amine-coated surfaces in the absence of serum.[60]

3.4. Cell Proliferation. Further cell culture studies aiming to assess cell behavior on the different plasma-treated scaffolds were performed on scaffolds preincubated and seeded in (+)FBS to have a comparable cell number and distribution among scaffolds, as these parameters can influence cell behavior on their own.[64] Initially, we confirmed that aging did not affect total cell attachment (Figure 7A) nor cell distribution (Figure S7), regardless of the plasma conditions. Plasma effect on cell adhesion and distribution also showed not to be hMSC donor dependent, suggesting the possibility of extrapolating our results to other hMSC populations (Figure S7B,C). Interestingly, hMSCs did not proliferate significantly after 7 days of culture, neither on untreated nor on fresh or aged plasma scaffolds (Figure 7B). Despite this initial lack of proliferation, a significant increase in the DNA content with respect to day 1 was observed on all fresh and aged plasma-treated scaffolds after 14 days of culture (7 days in BM, followed by 7 days in MM) (Figure 7C). It is plausible that an increase in the available surface area, given by ECM production within the scaffold pore volume when cultured in MM, offered cells the possibility to further proliferate on plasma-treated scaffolds, as previously suggested.[4] Previous research also showed significant differences in proliferation among surface-functionalized and untreated 2D substrates only after long culture periods (~10 days),[25] whereas the use of dynamic culture systems or growth factors was found to be necessary to increase ECM production and boost cell proliferation on 3D plasma-treated scaffolds.[25,27] Notably, no differences in the hMSC proliferation rate were found among fresh scaffolds or aged scaffolds. However, while hMSCs in MA-VTMOS scaffolds proliferated at the same rate in fresh and aged scaffolds, higher levels in hMSC proliferation were found on fresh APTMS- and argon-treated scaffolds, compared to their aged counterparts. In the case of APTMS, this might be due to the lower density of functional groups and adsorbed proteins on aged scaffolds.

3.5. Osteogenic Differentiation Potential of hMSCs Seeded on Aged Plasma-Treated Scaffolds. The analysis of osteogenic differentiation was performed on aged scaffolds due to their higher applicability, as previously mentioned. Moreover, since comparable total cell numbers among conditions were observed at any time point evaluated during the culture on these scaffolds (Figure S8), it was then possible to focus solely on the influence of plasma activation and polymerization on differentiation and exclude the cell number and distribution-related effect on osteogenesis. Following this rationale, inefficiently seeded untreated control scaffolds were not included in the study. After seeding, scaffolds were cultured for a total of 54 days in MM (7 days in BM, followed by 47 days in MM). Immunofluorescence was used to evaluate collagen I deposition at early and late time points of the differentiation process (day 14 and 54). Representative fluorescence microscopy images in Figure 8A revealed that hMSCs were able to produce collagen I, one of the main bone ECM proteins, from early time points in all plasma-treated scaffold conditions. These images also revealed that ECM became denser and the pores were more filled in the course of the culture. Furthermore, the expression of relevant osteogenic genes was screened through PCR (Figure 8B) at 14 and 54

https://dx.doi.org/10.1021/acsami.0c19687
ACS Appl. Mater. Interfaces XXXX, XXX, XXX−XXX

days of culture. ALP, an early osteogenic marker, indicated no significant differences among plasma conditions or time points. Similarly, no statistical differences in OCN expression, a protein that bounds to hydroxyapatite, were found among plasma conditions and time points. RUNX2, a transcription factor modulating the expression of osteogenic proteins, was upregulated at day 54 in argon-treated scaffolds compared to other conditions. When analyzing osterix, bone sialoprotein and BMP2 gene expression, which are proteins present in a matured bone ECM, no upregulation was observed, except in argon-treated scaffolds at day 54 compared to day 14. However, no significant differences among plasma conditions were found at this time point. Overall, no clear trends were observed within this study and no plasma treatment showed to provide a distinct osteogenic stimulation to hMSCs over the others. In 2D functionalized surfaces, an enhanced osteogenic effect of amine groups compared to other functional groups has been correlated to the enhanced exposure of the integrin domain $\alpha5\beta1$ in adsorbed Fn and to high levels of recruitment of focal adhesion components and phosphorylation of focal adhesion kinases in the adhered cells, which are events required for osteoblast differentiation.[20−22,62,65] In this regard, it is plausible that aging masked the osteogenic stimulation potential of the APTMS surfaces and that some differences would have been evidenced under fresh conditions since APTMS fresh scaffolds displayed the highest levels of protein adsorption and, potentially, of integrin domain $\alpha5\beta1$. It is also possible that the effect of surface chemistry is only pronounced at an early stage when cells are in direct contact with the scaffold surface and that upon ECM production by cells during longer-term culture, cell−plasma treated substrate contact becomes limited and ineffective.[66] Nevertheless, due to the lack of published reports simultaneously comparing the effect of different surface chemistries on osteogenic differentiation in 3D scaffolds, comparing our results with previous literature becomes challenging. To the best of our knowledge, a single study as such has demonstrated that salt-leached poly(carbonate-urea) urethane scaffolds modified by allylamine plasma polymerization significantly enhanced osteogenic differentiation of adipose-derived stem cells compared to carboxylic acid-modified scaffolds.[67] However, no clear explanation of how the amine group affected the osteogenesis pathway was reported. Moreover, since these scaffolds were fabricated by a conventional manufacturing method, i.e. porogen leaching, the poor interconnected porosity might have induced a different cell behavior compared to what we observed in ME-AM scaffolds.

Besides, it is worth noticing that ECM mineralization was not observed in any scaffold type during the evaluated culture period (Figure S9A), despite the proven mineralization potential of these cells in 2D (Figure S9B). Also, no matrix mineralization was attained on fresh scaffolds (Figure S9C). Thus, it is believed that cells on the scaffolds did not reach a mature level of differentiation yet, and that the homogenous cell distribution after seeding given by bioactive surface chemistry is not sufficient for a successful osteogenic differentiation and mineralization outcome. It is hypothesized that larger cell seeding numbers could have led to larger cell attachment and, therefore, higher cell density and cell−cell contact for accelerated differentiation.[68−70] To investigate this, preliminary experiments were conducted, in which scaffolds were seeded with a larger seeding density (400 000 cells per scaffold (400k), instead of 200 000 (200k)). Despite higher cell seeding efficiency, as per DNA quantification (Figure S10A), cells in scaffolds seeded with 400k tended to form a denser monolayer in the scaffolds' bottom while maintaining the scaffolds' filaments as populated as when seeded with 200k (Figure S10B,C, day 1 of culture). However, some pores were already filled on the plasma-treated scaffolds seeded with 400k at day 7 (Figure S10D), a cell confluency level that was not observed with lower cell seeding density, and that could potentially derive in earlier osteogenesis. Future work will be aimed at understanding if an enhancement of cell confluency at earlier time points, at the expense of needing a larger cell stock, might lead to mineralization and tissue maturation. This will help us to unravel if specific plasma-induced surface chemistry can offer enhanced osteogenic differentiation or if, on the contrary, cell confluency regardless of the surface chemistry is the primary parameter effectively playing a role in osteogenic differentiation on 3D-AM scaffolds.

4. CONCLUSIONS

ME-AM enables the reproducible fabrication of highly porous polymeric scaffolds, ideal for tissue regeneration. However, the lack of cell adhesion sites on synthetic polymers hinders an efficient cell adhesion to the scaffolds, the first step toward the development of a functional construct. The aim of this study was to fabricate 3D scaffolds using a hybrid AM technique that enabled scaffold fabrication by ME-AM and their subsequent APPJ treatment to enhance their bioactivity within the same platform. While argon activation resulted in an unspecific surface plasma treatment, APTMS plasma polymerization enabled the deposition of a positively charged coating containing amine functional groups, and MA-VTMOS rendered the surface of the scaffold negatively charged by depositing carboxyl and anhydride functional groups. All plasma treatments increased the surface wettability of the scaffolds, enhanced cell-adhesive protein adsorption to their surface, and allowed for homogeneous cell attachment along the scaffold cross-section. Interestingly, cell attachment was found to be driven by cell−protein interactions in the presence of serum and by electrostatic interactions between the cell and the charged scaffold surface in serum-free conditions. This latter feature allowed for cell attachment and scaffold population on APTMS-treated scaffolds in the absence of serum, which possesses relevant clinical applications. Scaffold storage led to the aging of the surface treatment, in terms of a slight reduction of exposed functional groups. However, cell attachment and proliferation were not significantly affected. Notably, none of the plasma treatments stimulated osteogenic differentiation of hMSCs significantly more than the others. It is hypothesized that initial cell confluency might play a major role, overruling the effects of specific surface chemistry on the osteogenic differentiation of hMSCs and ECM mineralization on 3D ME-AM scaffolds. Overall, this newly proposed method enabled an efficient workflow of scaffold production and surface treatment and opens the door to future research on the effect of different plasma treatments on cell behavior on 3D ME-AM scaffolds.

■ ASSOCIATED CONTENT

Supporting Information

The Supporting Information is available free of charge at https://pubs.acs.org/doi/10.1021/acsami.0c19687.

https://dx.doi.org/10.1021/acsami.0c19687
ACS Appl. Mater. Interfaces XXXX, XXX, XXX−XXX

Hybrid additive manufacturing platform (Figure S1); staining specificity and staining of ethanol disinfected scaffolds (Figure S2); ζ potential measurements (Figure S3); regions of interest of FTIR spectra (Figure S4); SEM of fresh plasma-treated scaffolds (Figure S5); fluorescence images of cell coverage on fresh scaffolds' bottom sides (Figure S6); fluorescence images of cell distribution and seeding efficiency quantification on aged scaffolds (Figure S7); DNA content on aged scaffolds over 54 days culture (Figure S8); alizarin red staining on plasma-treated scaffolds (Figure S9); and cell seeding efficiency quantification and fluorescence images of cell distribution on fresh scaffolds seeded with 400k and 200k cells (Figure S10) (PDF)

AUTHOR INFORMATION

Corresponding Author

Lorenzo Moroni − *Complex Tissue Regeneration Department, MERLN Institute for Technology-Inspired Regenerative Medicine, Maastricht University, 6229 ER Maastricht, The Netherlands;* orcid.org/0000-0003-1298-6025; Email: l.moroni@maastrichtuniversity.nl

Authors

Maria Cámara-Torres − *Complex Tissue Regeneration Department, MERLN Institute for Technology-Inspired Regenerative Medicine, Maastricht University, 6229 ER Maastricht, The Netherlands*

Ravi Sinha − *Complex Tissue Regeneration Department, MERLN Institute for Technology-Inspired Regenerative Medicine, Maastricht University, 6229 ER Maastricht, The Netherlands*

Paolo Scopece − *Nadir S.r.l., 30172 Venice, Italy;* orcid.org/0000-0003-1466-5823

Thomas Neubert − *Fraunhofer Institute for Surface Engineering and Thin Films IST, 38108 Braunschweig, Germany*

Kristina Lachmann − *Fraunhofer Institute for Surface Engineering and Thin Films IST, 38108 Braunschweig, Germany*

Alessandro Patelli − *Department of Physics and Astronomy, Padova University, 35131 Padova, Italy;* orcid.org/0000-0001-7662-4352

Carlos Mota − *Complex Tissue Regeneration Department, MERLN Institute for Technology-Inspired Regenerative Medicine, Maastricht University, 6229 ER Maastricht, The Netherlands;* orcid.org/0000-0001-5935-6245

Complete contact information is available at: https://pubs.acs.org/10.1021/acsami.0c19687

Author Contributions

M.C.-T., R.S., C.M., and L.M. conceived the idea. M.C.-T. and R.S. prepared the samples. M.C.T. designed and executed the experiments, and analyzed the results. P.S. and A.P. developed the plasma torch. T.N. and K.L. contributed to data analysis. A.P., C.M., and L.M. supervised the project. All authors wrote, revised, and approved the manuscript.

Notes

The authors declare no competing financial interest.

ACKNOWLEDGMENTS

We are grateful to the FAST project funded under the H2020-NMP-PILOTS-2015 scheme (GA no. 685825) for financial support. Some of the materials used in this work were provided by the Texas A&M Health Science Center College of Medicine Institute for Regenerative Medicine at Scott & White through a grant from NCRR of the NIH (Grant #P40RR017447).

REFERENCES

(1) Mota, C.; Puppi, D.; Chiellini, F.; Chiellini, E. Additive Manufacturing Techniques for the Production of Tissue Engineering Constructs. *J. Tissue Eng. Regener. Med.* **2015**, *9*, 174−190.

(2) Kim, K.; Dean, D.; Mikos, A. G.; Fisher, J. P. Effect of Initial Cell Seeding Density on Early Osteogenic Signal Expression of Rat Bone Marrow Stromal Cells Cultured on Cross-Linked Poly(Propylene Fumarate) Disks. *Biomacromolecules* **2009**, *10*, 1810−1817.

(3) Hasegawa, T.; Miwa, M.; Sakai, Y.; Niikura, T.; Lee, S. Y.; Oe, K.; Iwakura, T.; Kurosaka, M.; Komori, T. Efficient Cell-Seeding into Scaffolds Improves Bone Formation. *J. Dent. Res.* **2010**, *89*, 854−859.

(4) Cámara-Torres, M.; Sinha, R.; Mota, C.; Moroni, L. Improving Cell Distribution on 3d Additive Manufactured Scaffolds through Engineered Seeding Media Density and Viscosity. *Acta Biomater.* **2020**, *101*, 183−195.

(5) Chen, Y.; Bloemen, V.; Impens, S.; Moesen, M.; Luyten, F. P.; Schrooten, J. Characterization and Optimization of Cell Seeding in Scaffolds by Factorial Design: Quality by Design Approach for Skeletal Tissue Engineering. *Tissue Eng., Part C* **2011**, *17*, 1211−1221.

(6) Sobral, J. M.; Caridade, S. G.; Sousa, R. A.; Mano, J. F.; Reis, R. L. Three-Dimensional Plotted Scaffolds with Controlled Pore Size Gradients: Effect of Scaffold Geometry on Mechanical Performance and Cell Seeding Efficiency. *Acta Biomater.* **2011**, *7*, 1009−1018.

(7) Leferink, A. M.; Hendrikson, W.; Rouwkema, J.; Karperien, M.; van Blitterswijk, C.; Moroni, L. Increased Cell Seeding Efficiency in Bioplotted Three-Dimensional Peot/Pbt Scaffolds. *J. Tissue Eng. Regener. Med.* **2016**, *10*, 679−689.

(8) Dong, L.; Wang, S.-J.; Zhao, X.-R.; Zhu, Y.-F.; Yu, J.-K. 3d-Printed Poly(E-Caprolactone) Scaffold Integrated with Cell-Laden Chitosan Hydrogels for Bone Tissue Engineering. *Sci. Rep.* **2017**, *7*, No. 13412.

(9) Whitely, M.; Cereceres, S.; Dhavalikar, P.; Salhadar, K.; Wilems, T.; Smith, B.; Mikos, A.; Cosgriff-Hernandez, E. Improved in Situ Seeding of 3d Printed Scaffolds Using Cell-Releasing Hydrogels. *Biomaterials* **2018**, *185*, 194−204.

(10) Ostrowska, B.; Di Luca, A.; Moroni, L.; Swieszkowski, W. Influence of Internal Pore Architecture on Biological and Mechanical Properties of Three-Dimensional Fiber Deposited Scaffolds for Bone Regeneration. *J. Biomed. Mater. Res., Part A* **2016**, *104*, 991−1001.

(11) Yu, J.; Xu, Y.; Li, S.; Seifert, G. V.; Becker, M. L. Three-Dimensional Printing of Nano Hydroxyapatite/Poly(Ester Urea) Composite Scaffolds with Enhanced Bioactivity. *Biomacromolecules* **2017**, *18*, 4171−4183.

(12) Qi, X.; Pei, P.; Zhu, M.; Du, X.; Xin, C.; Zhao, S.; Li, X.; Zhu, Y. Three Dimensional Printing of Calcium Sulfate and Mesoporous Bioactive Glass Scaffolds for Improving Bone Regeneration in Vitro and in Vivo. *Sci. Rep.* **2017**, *7*, No. 42556.

(13) Wang, W.; Caetano, G.; Ambler, W. S.; Blaker, J. J.; Frade, M. A.; Mandal, P.; Diver, C.; Bartolo, P. Enhancing the Hydrophilicity and Cell Attachment of 3d Printed Pcl/Graphene Scaffolds for Bone Tissue Engineering. *Materials* **2016**, *9*, No. 992.

(14) Zamani, Y.; Mohammadi, J.; Amoabediny, G.; Visscher, D. O.; Helder, M. N.; Zandieh-Doulabi, B.; Klein-Nulend, J. Enhanced Osteogenic Activity by Mc3t3-E1 Pre-Osteoblasts on Chemically Surface-Modified Poly(E-Caprolactone) 3d-Printed Scaffolds Compared to Rgd Immobilized Scaffolds. *Biomed. Mater.* **2018**, *14*, No. 015008.

(15) Kosik-Kozioł, A.; Graham, E.; Jaroszewicz, J.; Chlanda, A.; Kumar, P. T. S.; Ivanovski, S.; Święszkowski, W.; Vaquette, C. Surface Modification of 3d Printed Polycaprolactone Constructs Via a Solvent

https://dx.doi.org/10.1021/acsami.0c19687
ACS Appl. Mater. Interfaces XXXX, XXX, XXX−XXX

Treatment: Impact on Physical and Osteogenic Properties. *ACS Biomater. Sci. Eng.* **2019**, *5*, 318−328.
(16) Kang, S.-W.; Kim, J.-S.; Park, K.-S.; Cha, B.-H.; Shim, J.-H.; Kim, J. Y.; Cho, D.-W.; Rhie, J.-W.; Lee, S.-H. Surface Modification with Fibrin/Hyaluronic Acid Hydrogel on Solid-Free Form-Based Scaffolds Followed by Bmp-2 Loading to Enhance Bone Regeneration. *Bone* **2011**, *48*, 298−306.
(17) De Geyter, N.; Morent, R. Cold Plasma Surface Modification of Biodegradable Polymer Biomaterials. In *Biomaterials for Bone Regeneration*; Dubruel, P.; Van Vlierberghe, S., Eds.; Woodhead Publishing, 2014; Chapter 7, pp 202−224.
(18) Barrias, C. C.; Martins, M. C. L.; Almeida-Porada, G.; Barbosa, M. A.; Granja, P. L. The Correlation between the Adsorption of Adhesive Proteins and Cell Behaviour on Hydroxyl-Methyl Mixed Self-Assembled Monolayers. *Biomaterials* **2009**, *30*, 307−316.
(19) Arima, Y.; Iwata, H. Preferential Adsorption of Cell Adhesive Proteins from Complex Media on Self-Assembled Monolayers and Its Effect on Subsequent Cell Adhesion. *Acta Biomater.* **2015**, *26*, 72−81.
(20) Keselowsky, B. G.; Collard, D. M.; García, A. J. Surface Chemistry Modulates Focal Adhesion Composition and Signaling through Changes in Integrin Binding. *Biomaterials* **2004**, *25*, 5947−5954.
(21) Curran, J. M.; Chen, R.; Hunt, J. A. The Guidance of Human Mesenchymal Stem Cell Differentiation in Vitro by Controlled Modifications to the Cell Substrate. *Biomaterials* **2006**, *27*, 4783−4793.
(22) Chen, M.; Zhang, Y.; Zhou, Y.; Zhang, Y.; Lang, M.; Ye, Z.; Tan, W.-S. Pendant Small Functional Groups on Poly(ϵ-Caprolactone) Substrate Modulate Adhesion, Proliferation and Differentiation of Human Mesenchymal Stem Cells. *Colloids Surf., B* **2015**, *134*, 322−331.
(23) Yildirim, E. D.; Besunder, R.; Pappas, D.; Allen, F.; Guceri, S.; Sun, W. Accelerated Differentiation of Osteoblast Cells on Polycaprolactone Scaffolds Driven by a Combined Effect of Protein Coating and Plasma Modification. *Biofabrication* **2010**, *2*, No. 014109.
(24) Jeon, H.; Lee, H.; Kim, G. A Surface-Modified Poly(ϵ-Caprolactone) Scaffold Comprising Variable Nanosized Surface-Roughness Using a Plasma Treatment. *Tissue Eng., Part C* **2014**, *20*, 951−963.
(25) Lerman, M. J.; Smith, B. T.; Gerald, A. G.; Santoro, M.; Fookes, J. A.; Mikos, A. G.; Fisher, J. P. Aminated 3d Printed Polystyrene Maintains Stem Cell Proliferation and Osteogenic Differentiation. *Tissue Eng., Part C* **2020**, *26*, 118−131.
(26) Domingos, M.; Intranuovo, F.; Gloria, A.; Gristina, R.; Ambrosio, L.; Bártolo, P. J.; Favia, P. Improved Osteoblast Cell Affinity on Plasma-Modified 3-D Extruded Pcl Scaffolds. *Acta Biomater.* **2013**, *9*, 5997−6005.
(27) Cools, P.; Mota, C.; Lorenzo-Moldero, I.; Ghobeira, R.; De Geyter, N.; Moroni, L.; Morent, R. Acrylic Acid Plasma Coated 3d Scaffolds for Cartilage Tissue Engineering Applications. *Sci. Rep.* **2018**, *8*, No. 3830.
(28) Cools, P.; Sainz-García, E.; Geyter, N. D.; Nikiforov, A.; Blajan, M.; Shimizu, K.; Alba-Elías, F.; Leys, C.; Morent, R. Influence of Dbd Inlet Geometry on the Homogeneity of Plasma-Polymerized Acrylic Acid Films: The Use of a Microplasma−Electrode Inlet Configuration. *Plasma Processes Polym.* **2015**, *12*, 1153−1163.
(29) De Geyter, N.; Morent, R.; Leys, C. Penetration of a Dielectric Barrier Discharge Plasma into Textile Structures at Medium Pressure. *Plasma Sources Sci. Technol.* **2006**, *15*, 78.
(30) Lu, X.; Laroussi, M.; Puech, V. On Atmospheric-Pressure Non-Equilibrium Plasma Jets and Plasma Bullets. *Plasma Sources Sci. Technol.* **2012**, *21*, No. 034005.
(31) Liu, F.; Wang, W.; Hinduja, S.; Bártolo, P. J. Hybrid Additive Manufacturing System for Zonal Plasma-Treated Scaffolds. *3D Print. Addit. Manuf.* **2018**, *5*, 205−213.
(32) Sinha, R.; Cámara-Torres, M.; Scopece, P.; Verga Falzacappa, E.; Patelli, A.; Moroni, L.; Mota, C. A Hybrid Additive Manufacturing Platform to Create Bulk and Surface Composition Gradients on Scaffolds for Tissue Regeneration. *Nat. Commun.* **2021**.
(33) Hody, H.; Choquet, P.; Moreno-Couranjou, M.; Maurau, R.; Pireaux, J.-J. Optimization of Carboxyl Surface Functionalization by Ma-Vtms Copolymerization Using Atmospheric Pressure Plasma Dbd: Influence of the Carrier Gas. *Plasma Processes Polym.* **2010**, *7*, 403−410.
(34) Chen, Z.; Zhao, J.; Jin, C.; Yuan, Y.; Zhang, Y.; Tatoulian, M.; Rao, X. Plasma Deposited Aptes: A Potential Film for Biomedical Application. *Mater. Lett.* **2020**, *264*, No. 127350.
(35) Bitar, R.; Cools, P.; De Geyter, N.; Morent, R. Acrylic Acid Plasma Polymerization for Biomedical Use. *Appl. Surf. Sci.* **2018**, *448*, 168−185.
(36) Bulou, S.; Lecoq, E.; Loyer, F.; Frache, G.; Fouquet, T.; Gueye, M.; Belmonte, T.; Choquet, P. Study of a Pulsed Post-Discharge Plasma Deposition Process of Aptes: Synthesis of Highly Organic Pp-Aptes Thin Films with Nh2 Functionalized Polysilsesquioxane Evidences. *Plasma Processes Polym.* **2019**, *16*, No. 1800177.
(37) Patelli, A.; Verga Falzacappa, E.; Scopece, P.; Pierobon, R.; Vezzu', S. Method for Generating Atmospheric Plasma Jet and Atmospheric Plasma Mini-Torch Device. JP6569954B2, 2015.
(38) Manakhov, A.; Moreno-Couranjou, M.; Boscher, N. D.; Rogé, V.; Choquet, P.; Pireaux, J.-J. Atmospheric Pressure Pulsed Plasma Copolymerisation of Maleic Anhydride and Vinyltrimethoxysilane: Influence of Electrical Parameters on Chemistry, Morphology and Deposition Rate of the Coatings. *Plasma Processes Polym.* **2012**, *9*, 435−445.
(39) Zanini, S.; Grimoldi, E.; Riccardi, C. Development of Controlled Releasing Surfaces by Plasma Deposited Multilayers. *Mater. Chem. Phys.* **2013**, *138*, 850−855.
(40) Thomas, M.; von Hausen, M.; Klages, C.-P.; Baumhof, P. Generation of Stable Coatings with Carboxylic Groups by Copolymerization of Maa and Vtms Using Dbd at Atmospheric Pressure. *Plasma Processes Polym.* **2007**, *4*, S475−S481.
(41) Patelli, A.; Mussano, F.; Brun, P.; Genova, T.; Ambrosi, E.; Michieli, N.; Mattei, G.; Scopece, P.; Moroni, L. Nanoroughness, Surface Chemistry, and Drug Delivery Control by Atmospheric Plasma Jet on Implantable Devices. *ACS Appl. Mater. Interfaces* **2018**, *10*, 39512−39523.
(42) Lecoq, E.; Duday, D.; Bulou, S.; Frache, G.; Hilt, F.; Maurau, R.; Choquet, P. Plasma Polymerization of Aptes to Elaborate Nitrogen Containing Organosilicon Thin Films: Influence of Process Parameters and Discussion About the Growing Mechanisms. *Plasma Processes Polym.* **2013**, *10*, 250−261.
(43) Mostofi Sarkari, N.; Doğan, Ö.; Bat, E.; Mohseni, M.; Ebrahimi, M. Assessing Effects of (3-Aminopropyl)Trimethoxysilane Self-Assembled Layers on Surface Characteristics of Organosilane-Grafted Moisture-Crosslinked Polyethylene Substrate: A Comparative Study between Chemical Vapor Deposition and Plasma-Facilitated in Situ Grafting Methods. *Appl. Surf. Sci.* **2019**, *497*, No. 143751.
(44) Damanik, F. F. R.; Rothuizen, T. C.; van Blitterswijk, C.; Rotmans, J. I.; Moroni, L. Towards an in Vitro Model Mimicking the Foreign Body Response: Tailoring the Surface Properties of Biomaterials to Modulate Extracellular Matrix. *Sci. Rep.* **2015**, *4*, No. 6325.
(45) Cools, P.; Asadian, M.; Nicolaus, W.; Declercq, H.; Morent, R.; De Geyter, N. Surface Treatment of Peot/Pbt (55/45) with a Dielectric Barrier Discharge in Air, Helium, Argon and Nitrogen at Medium Pressure. *Materials* **2018**, *11*, No. 391.
(46) Olde Riekerink, M. B.; Claase, M. B.; Engbers, G. H. M.; Grijpma, D. W.; Feijen, J. Gas Plasma Etching of Peo/Pbt Segmented Block Copolymer Films. *J. Biomed. Mater. Res., Part A* **2003**, *65A*, 417−428.
(47) Cao, B.; Peng, Y.; Liu, X.; Ding, J. Effects of Functional Groups of Materials on Nonspecific Adhesion and Chondrogenic Induction of Mesenchymal Stem Cells on Free and Micropatterned Surfaces. *ACS Appl. Mater. Interfaces* **2017**, *9*, 23574−23585.
(48) Nakamatsu, J.; Delgado-Aparicio, L. F.; Da Silva, R.; Soberon, F. Ageing of Plasma-Treated Poly(Tetrafluoroethylene) Surfaces. *J. Adhes. Sci. Technol.* **1999**, *13*, 753−761.

https://dx.doi.org/10.1021/acsami.0c19687
ACS Appl. Mater. Interfaces XXXX, XXX, XXX−XXX

(49) Borris, J.; Thomas, M.; Klages, C.-P.; Faupel, F.; Zaporojtchenko, V. Investigations into Composition and Structure of Dbd-Deposited Amino Group Containing Polymer Layers. *Plasma Processes Polym.* **2007**, *4*, S482−S486.
(50) Banik, I.; Kim, K. S.; Yun, Y. I.; Kim, D. H.; Ryu, C. M.; Park, C. S.; Sur, G. S.; Park, C. E. A Closer Look into the Behavior of Oxygen Plasma-Treated High-Density Polyethylene. *Polymer* **2003**, *44*, 1163−1170.
(51) Kim, K. S.; Ryu, C. M.; Park, C. S.; Sur, G. S.; Park, C. E. Investigation of Crystallinity Effects on the Surface of Oxygen Plasma Treated Low Density Polyethylene Using X-Ray Photoelectron Spectroscopy. *Polymer* **2003**, *44*, 6287−6295.
(52) Morent, R.; De Geyter, N.; Leys, C.; Gengembre, L.; Payen, E. Study of the Ageing Behaviour of Polymer Films Treated with a Dielectric Barrier Discharge in Air, Helium and Argon at Medium Pressure. *Surf. Coat. Technol.* **2007**, *201*, 7847−7854.
(53) Arima, Y.; Iwata, H. Effects of Surface Functional Groups on Protein Adsorption and Subsequent Cell Adhesion Using Self-Assembled Monolayers. *J. Mater. Chem.* **2007**, *17*, 4079−4087.
(54) Arima, Y.; Iwata, H. Effect of Wettability and Surface Functional Groups on Protein Adsorption and Cell Adhesion Using Well-Defined Mixed Self-Assembled Monolayers. *Biomaterials* **2007**, *28*, 3074−3082.
(55) Lin, J.-H.; Chang, H.-Y.; Kao, W.-L.; Lin, K.-Y.; Liao, H.-Y.; You, Y.-W.; Kuo, Y.-T.; Kuo, D.-Y.; Chu, K.-J.; Chu, Y.-H.; Shyue, J.-J. Effect of Surface Potential on Extracellular Matrix Protein Adsorption. *Langmuir* **2014**, *30*, 10328−10335.
(56) Hoshiba, T.; Yoshikawa, C.; Sakakibara, K. Characterization of Initial Cell Adhesion on Charged Polymer Substrates in Serum-Containing and Serum-Free Media. *Langmuir* **2018**, *34*, 4043−4051.
(57) Khang, D.; Kim, S. Y.; Liu-Snyder, P.; Palmore, G. T. R.; Durbin, S. M.; Webster, T. J. Enhanced Fibronectin Adsorption on Carbon Nanotube/Poly(Carbonate) Urethane: Independent Role of Surface Nano-Roughness and Associated Surface Energy. *Biomaterials* **2007**, *28*, 4756−4768.
(58) Webb, K.; Hlady, V.; Tresco, P. A. Relative Importance of Surface Wettability and Charged Functional Groups on Nih 3t3 Fibroblast Attachment, Spreading, and Cytoskeletal Organization. *J. Biomed. Mater. Res.* **1998**, *41*, 422−430.
(59) Chang, H.-Y.; Kao, W.-L.; You, Y.-W.; Chu, Y.-H.; Chu, K.-J.; Chen, P.-J.; Wu, C.-Y.; Lee, Y.-H.; Shyue, J.-J. Effect of Surface Potential on Epithelial Cell Adhesion, Proliferation and Morphology. *Colloids Surf., B* **2016**, *141*, 179−186.
(60) Massia, S. P.; Hubbell, J. A. Immobilized Amines and Basic Amino Acids as Mimetic Heparin-Binding Domains for Cell Surface Proteoglycan-Mediated Adhesion. *J. Biol. Chem.* **1992**, *267*, 10133−10141.
(61) Wang, M.; Favi, P.; Cheng, X.; Golshan, N. H.; Ziemer, K. S.; Keidar, M.; Webster, T. J. Cold Atmospheric Plasma (Cap) Surface Nanomodified 3d Printed Polylactic Acid (Pla) Scaffolds for Bone Regeneration. *Acta Biomater.* **2016**, *46*, 256−265.
(62) Griffin, M. F.; Ibrahim, A.; Seifalian, A. M.; Butler, P. E. M.; Kalaskar, D. M.; Ferretti, P. Chemical Group-Dependent Plasma Polymerisation Preferentially Directs Adipose Stem Cell Differentiation Towards Osteogenic or Chondrogenic Lineages. *Acta Biomater.* **2017**, *50*, 450−461.
(63) Griffin, M.; Palgrave, R.; Baldovino-Medrano, V. G.; Butler, P. E.; Kalaskar, D. M. Argon Plasma Improves the Tissue Integration and Angiogenesis of Subcutaneous Implants by Modifying Surface Chemistry and Topography. *Int. J. Nanomed.* **2018**, *13*, 6123.
(64) Lode, A.; Bernhardt, A.; Gelinsky, M. Cultivation of Human Bone Marrow Stromal Cells on Three-Dimensional Scaffolds of Mineralized Collagen: Influence of Seeding Density on Colonization, Proliferation and Osteogenic Differentiation. *J. Tissue Eng. Regener. Med.* **2008**, *2*, 400−407.
(65) Moursi, A. M.; Globus, R. K.; Damsky, C. H. Interactions between Integrin Receptors and Fibronectin Are Required for Calvarial Osteoblast Differentiation in Vitro. *J. Cell Sci.* **1997**, *110*, 2187−2196.
(66) Wang, P.-Y.; Clements, L. R.; Thissen, H.; Tsai, W.-B.; Voelcker, N. H. Screening Rat Mesenchymal Stem Cell Attachment and Differentiation on Surface Chemistries Using Plasma Polymer Gradients. *Acta Biomater.* **2015**, *11*, 58−67.
(67) Griffin, M. F.; Ibrahim, A.; Seifalian, A. M.; Butler, P. E. M.; Kalaskar, D. M.; Ferretti, P. Chemical Group-Dependent Plasma Polymerisation Preferentially Directs Adipose Stem Cell Differentiation Towards Osteogenic or Chondrogenic Lineages. *Acta Biomater.* **2017**, *50*, 450−461.
(68) Holy, C. E.; Shoichet, M. S.; Davies, J. E. Engineering Three-Dimensional Bone Tissue in Vitro Using Biodegradable Scaffolds: Investigating Initial Cell-Seeding Density and Culture Period. *J. Biomed. Mater. Res.* **2000**, *51*, 376−382.
(69) Noda, S.; Kawashima, N.; Yamamoto, M.; Hashimoto, K.; Nara, K.; Sekiya, I.; Okiji, T. Effect of Cell Culture Density on Dental Pulp-Derived Mesenchymal Stem Cells with Reference to Osteogenic Differentiation. *Sci. Rep.* **2019**, *9*, No. 5430.
(70) Abo-Aziza, F. A. M.; Zaki, A. A. The Impact of Confluence on Bone Marrow Mesenchymal Stem (Bmmsc) Proliferation and Osteogenic Differentiation. *Int. J. Hematol.−Oncol. Stem Cell Res.* **2017**, *11*, 121−132.

https://dx.doi.org/10.1021/acsami.0c19687
ACS Appl. Mater. Interfaces XXXX, XXX, XXX−XXX